Electron Tunneling and *ab Initio* Calculations Related to the One-Electron Oxidation of NAD(P)H Bound to Catalase†

Leif P. Olson and Thomas C. Bruice*

Department of Chemistry, University of California at Santa Barbara, Santa Barbara, California 93106

Received December 14, 1994; Revised Manuscript Received March 21, 1995⊗

ABSTRACT: Models for NAD(P)H $1e^-$ oxidation in bovine catalase were studied using Hartree−Fock *ab initio* calculations, along with information taken from the published X-ray structure of the enzyme. Geometries and energies of ground states and transition states were calculated at the 6-31G* level for *N*-methyl-1,4-dihydropyridine and *N*-methyl-1,4-dihydronicotinamide undergoing the pathway (i) $1e^-$ oxidation to yield the radical cation, (ii) general-base-catalyzed (hydroxide and/or imidazole) deprotonation of the radical cation to yield the neutral radical, and (iii) $1e^-$ oxidation of the neutral radical to the *N*-methylpyridinium or *N*-methylnicotinamide cation. Barrier heights for deprotonation of the radical cation intermediates were calculated to be 7−11 kcal/mol. Kinetic isotope effects were calculated for general-base-catalyzed deprotonation of the *N*-methyl-1,4-dihydropyridine radical cation and the 4,4-dideuterio species and found to be $k_H/k_{D2} = 5.38$ (hydroxide) or 3.64 (imidazole), in qualitative agreement with published experimental isotope effects for the analogous deprotonation of *N*-methyl-1,10-dihydroacridan or the *N*-methyl-1,10-dideuterioacridan radical cation. In the calculated transition state for imidazole deprotonation of the *N*-methyl-1,4-dihydronicotinamide radical cation, an unusual short contact was calculated and interpreted as a hydrogen bond (2.35 Å) between the amide oxygen and the hydrogen attached to C2 of imidazole. Similar hydrogen bonds were also observed and calculated at the 3-21G and 6-31G* levels between His234 of catalase and the amide oxygen of bound NAD(P)H and complexes of *N,N'*-dimethyl-1,4-dihydronicotinamide or *cis*-*N*-methylformamide with *N*-methylimidazole. Comparison of these results to the X-ray structure of bovine catalase allows for further interpretation of the possible roles of the imidazole bases His234 and His304 and the hydrogen-bonded contacts in the NAD(P)H binding site. Electron tunneling pathways between NAD(P)H and the iron protoporphyrin IX (PP-IX) axial tyrosinate ligand Tyr357 in molecular dynamics and X-ray crystal structures of bovine catalase were calculated using PATHWAYS II (version 2.01). The pathways which were calculated included those involving the amino acid residue Tyr214, which is near the NAD(P)H binding site. Coupling involving Tyr357 was not particularly efficient; however, strong coupling between Tyr214 and iron-protoporphyrin IX was observed. These pathways may be important if electron transfer is stepwise; i.e., Tyr214 oxidized first, followed by NAD(P)H.

Catalase efficiently catalyzes the disproportionation of hydrogen peroxide to water and dioxygen (eq 1a,b) (Schonbaum & Boyer, 1976). The (protoporphyrin IX)iron(III) at the active site reacts with hydrogen peroxide to give a hypervalent iron porphyrin species (compound **I**) and a molecule of water through what is overall a heterolytic scission of the peroxide O−O bond (eq 1a). Compound **I**

$$\text{catalase}-(\text{porph})\text{Fe}^{\text{III}} + \text{H}_2\text{O}_2 \rightarrow \text{compound I} + \text{H}_2\text{O} \quad (1a)$$

$$\text{compound I} + \text{H}_2\text{O}_2 \rightarrow \text{catalase}-(\text{porph})\text{Fe}^{\text{III}} + \text{H}_2\text{O} + \text{O}_2 \quad (1b)$$

$$\text{compound I} + \text{CH}_3\text{CH}_2\text{OH} \rightarrow \text{catalase}-(\text{porph})\text{Fe}^{\text{III}} + \text{H}_2\text{O} + \text{CH}_3\text{CHO} \quad (2)$$

(Schonbaum & Boyer, 1976) is 2 oxidation equivalents above the resting (protoporphyrin IX) iron(III) state and has been suggested by a variety of spectroscopic methods (Dolphin *et al.*, 1971; Moss *et al.*, 1969; Schulz *et al.*, 1979; Roberts *et al.*, 1981) to be an iron(IV) oxo porphyrin π-cation radical. Other studies suggest that at least part of the electron deficiency resides on the axial protein ligand attached to the heme iron in compound I of peroxidases (Chuang & van Wart, 1992; Thanabal *et al.*, 1988; Fujita *et al.*, 1983). Compound **I** is the active oxidant, which reacts with another molecule of H_2O_2 to give dioxygen and water (eq 1b) or oxidizes another small substrate molecule. Compound **I** reacts, for example, with ethanol to give acetaldehyde (eq 2) (Schonbaum, 1976). A second hypervalent iron porphyrin species, compound **II**, can form *via* one-electron reduction of compound **I**, and it is an iron(IV) oxo ligated porphyrin (eq 3). The electron for the reduction may originate in the

$$\text{compound I} + 1e^- \rightarrow \underset{\text{compound II}}{\text{catalase}-(\text{porph})\text{Fe}^{\text{IV}}=\text{O}} \quad (3)$$

protein matrix surrounding the iron porphyrin cofactor, with Tyr357 (ligated to the iron) suggested (Hillar *et al.*, 1994) as the possible donor in bovine catalase. Compound **II** does not take part in the catalytic cycle of the reaction of catalase

† Financial support was provided by the National Institutes of Health and the Office of Naval Research. We thank the San Diego Supercomputer Center for grants of supercomputer time.

⊗ Abstract published in *Advance ACS Abstracts,* May 15, 1995.

0006-2960/95/0434-7335$09.00/0

with hydrogen peroxide, and its accumulation leads to inactivation of the enzyme.

Kirkman and Gaetani (1984) discovered the presence of tightly bound 1,4-dihydronicotinamide adenine dinucleotide 2′-phosphate [(NAD(P)H)][1] in bovine catalase. Reevaluation of the high-resolution (2.5 Å) X-ray structure for bovine catalase unequivocally established the presence of NAD(P)H in each subunit of the tetrameric protein (Murthy *et al.*, 1981; Fita & Rossmann, 1985). Subsequently, it has been shown (Kirkman & Gaetani, 1984; Jouve *et al.*, 1989; Melik-Adamyan *et al.*, 1986; Hillar *et al.*, 1994) that human erythrocyte, canine, *Proteus mirabilis*, *Micrococcus lysodeikticus*, and yeast (A and T) catalases bind NAD(P)H; however, potato, *Escherichia coli*, *Aspergillus niger*, and *Penicillium vitale* catalases do not. Interestingly, the *P. vitale* catalase contains an additional "flavodoxin-like" domain (Melik-Adamyan *et al.*, 1986; Vainshtein *et al.*, 1986), suggesting the possibility of a role for a flavin cofactor in this species (although no FMN or FAD is observed in the X-ray structure and constitution studies with these cofactors have not been reported).

It has been suggested (Kirkman *et al.*, 1987; Almarsson *et al.*, 1993) that bound NAD(P)H plays a protective role, preventing the accumulation of compound **I** from damaging the enzyme and also preventing the inactivation of the enzyme by formation of compound **II**. Kirkman *et al.* (1987) and Hillar and Nicholls (Hillar & Nicholls, 1992; Hillar *et al.*, 1994) have reported that enzyme-bound NAD(P)H, while not reacting rapidly with compounds **I** or **II**, does react rapidly with an intermediate (possibly a highly unstable compound **II**−protein radical couple) in the pathway converting compound **I** to **II**. Kirkman *et al.* (1987) and our group (Almarsson *et al.*, 1993) have proposed a one-electron redox pathway (eq 4) whereby NAD(P)H is initially oxidized

$$\mathrm{NADPH} \underset{e^-}{\overset{-e^-}{\rightleftharpoons}} \mathrm{NADPH}^{\bullet+} \underset{H^+}{\overset{-H^+}{\rightleftharpoons}} \mathrm{NADP}^{\bullet} \xrightarrow{-e^-} \mathrm{NADP}^+ \quad (4)$$

to $NAD(P)H^{\bullet+}$. The $NAD(P)H^{\bullet+}$, after deprotonation to form $NADP^{\bullet}$, was proposed to deliver a second electron to either the iron atom or an exogenous oxidant such as O_2, forming $NADP^+$. Hillar and Nicholls (Hillar & Nicholls, 1992; Hillar *et al.*, 1994), on the other hand, reject the stepwise electron−proton−electron (EPE) pathway of Almarsson *et al.* (1993), claiming "it is unlikely that NAD(P)H will have the promiscuity" to react by other than a "concerted two-electron" pathway.

Figure 1 illustrates the difficulty faced by NAD(P)H in delivering reducing equivalents to the porphyrin, which is situated 13.7 Å from C4 of the dihydronicotinamide ring at its nearest point. This is too far for delivery of a hydride ion, so consideration of a concerted two-electron pathway must be abandoned in favor of a stepwise one-electron-transfer reduction pathway. In a recent demonstration of a

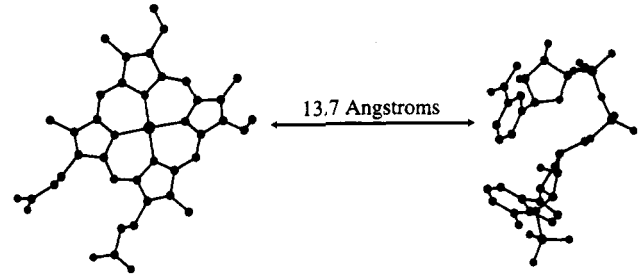

FIGURE 1: Spatial orientation of the iron-protoporphyrin IX and NAD(P)H cofactors in bovine catalase, taken from the X-ray crystal structure.

plausible EPE mechanistic scheme (Almarsson *et al.*, 1993), our group employed the catalase X-ray structure of Fita and Rossmann (1985), as well as structures calculated from the X-ray structure by molecular dynamics, to determine (i) probable pathways for electron tunneling through protein using the program PATHWAYS II (Regan, 1993) and (ii) probable enzyme functional groups which could play the required role of general bases for the intermediate deprotonation step in the EPE pathway. Figure 2 shows pathways for electron tunneling between the iron porphyrin and NAD(P)H, using the X-ray geometry (path A) or a calculated molecular dynamics geometry (path B) (Almarsson *et al.*, 1993) . Also in previous studies (Sinha & Bruice, 1984; Almarsson *et al.*, 1993), the rate constants and kinetic isotope effects for an EPE pathway were reported, using $Fe(CN)_6^{3-}$ as a model for compounds **I** and **II** and *N*-methyl-1,10-dihydroacridan as a model for NAD(P)H. The mechanistic importance of anisotropic puckering of the 1,4-dihydronicotinamide ring was explored (Almarsson *et al.*, 1993), using *ab initio* calculations, at the 3-21G* level.

Since that study appeared, it has been suggested (Hillar *et al.*, 1994) that certain tyrosine residues in catalase may facilitate electron transfer, as has been seen in a number of enzymes [e.g., Whittaker and Whittaker (1990), Barry and Babcock (1987), Kulmacz *et al.* (1987), and Graslund *et al.* (1982)]. Electron paramagnetic resonance spectroscopy and electron nuclear double resonance spectroscopy have established that tyrosine residues are oxidized to a radical (Bender *et al.*, 1989; Chandrasekhar *et al.*, 1986), centered on the phenolic moiety of tyrosine. Catalase may be an unusual case in that tyrosines might assist electron transfer in two different ways: (i) the electron deficiency of compound **I** of catalase may reside partially on the axial tyrosinate ligand (Tyr357 in bovine catalase) directly bonded to iron (Chuang & van Wart, 1992; Thanabal *et al.*, 1988; Fujita *et al.*, 1983), thereby connecting electron deficiency from the cofactor to protein; and (ii) other tyrosine residues may mediate long-range electron transfer by single-electron redox reactions.

This study is concerned with the EPE pathway and its further exploration using higher level *ab initio* calculations (including location of transition structures), and the role and mechanism of NAD(P)H bound to catalase. Alternative pathways for electron tunneling, where tyrosines are involved, are considered.

MATERIALS AND METHODS

Computational Methods. The calculations were performed using GAMESS (Schmidt *et al.*, 1993), Spartan 3.1 (Wavefunction, Inc., 1994), or Gaussian 92 (Frisch *et al.*, 1992)

[1] Abbreviations: EPE, electron−proton−electron; Im, imidazole; ImH^+, imidazolium ion; KIE, kinetic isotope effect; NADH, 1,4-dihydronicotinamide adenine dinucleotide; NAD(P)H, 1,4-dihydronicotinamide adenine dinucleotide 2′-phosphate; NicH, *N*-methyl-1,4-dihydronicotinamide; $NicH^{\bullet+}$, *N*-methyl-1,4-dihydronicotinamide radical cation; $Nic^{\bullet}$, *N*-methylnicotinamide radical; Nic^+, *N*-methylnicotinamide cation; PP-IX, protoporphyrin IX; PyH, *N*-methyl-1,4-dihydropyridine; $PyH^{\bullet+}$, *N*-methyl-1,4-dihydropyridine radical cation; $Py^{\bullet}$, *N*-methylpyridine radical; Py^+, *N*-methylpyridine cation; RHF, restricted Hartree−Fock; UHF, unrestricted Hartree−Fock.

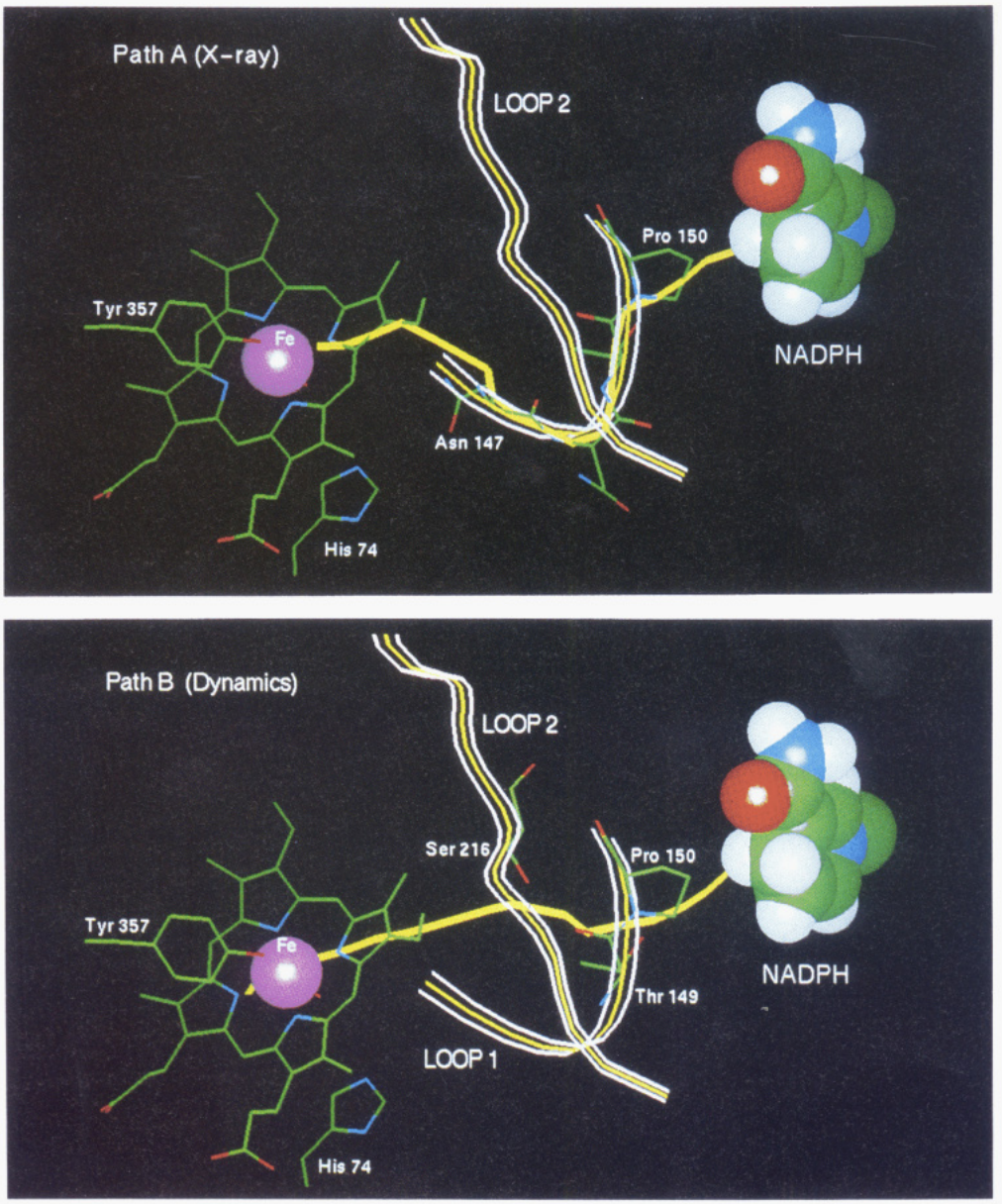

FIGURE 2: (a, top) Electron tunneling path A (Almarsson *et al.*, 1993) based on the X-ray crystal structure of bovine catalase: NADPH−jump−Pro150−Thr149−jump−Asn147−jump−CH_2=CH−(PP-IX pyrrole ring C)−Fe. (b, bottom) Electron tunneling path B (Almarsson *et al.*, 1993) based on a molecular dynamics average structure of bovine catalase: NADPH−jump−Pro150−Thr149−Hbond−Ser216−jump−CH_2=CH−(PP-IX pyrrole ring C)−Fe.

on Silicon Graphics Indigo and Indigo^2 or VAX 3100 workstations and using GAMESS and Gaussian 92 on the Cray C90 at the San Diego Supercomputer Center. Electron tunneling pathways were calculated using PATHWAYS II (version 2.01; Regan, 1993) on a Silicon Graphics 4D/340GTX workstation. Visualization of most structures and calculation of graphical surfaces were done using Spartan, which, in addition to its own *ab initio* module, can import files in the Brookhaven Protein Data Bank (pdb) format, among others. Using the NewZmat utility program associated with Gaussian 92, pdb files were created using nuclear coordinates from GAMESS or Gaussian 92 outputs when needed (this was unnecessary for structures calculated using Spartan). X-ray or *ab initio* structures were then visualized as desired, and after performing single-point quantum mechanical calculations within Spartan, graphical surfaces were created as well. Electron tunneling pathways were visualized using Insight II version 2.20 (Biosym Inc., 1992).

Ab Initio Methods. Most initial geometry searches were conducted at the AM1 semiempirical level (Dewar *et al.*, 1986) and then reoptimized using the 3-21G basis set [see Hehre *et al.* (1986) and Clark (1982) and references therein for a description of the basis sets used in this paper]. In most cases, final optimizations from the 3-21G structures were performed using the 6-31G* basis set. An unrestricted Hartree−Fock (UHF) wavefunction was used for all open-shell species. Singlet species were calculated using a restricted Hartree−Fock (RHF) wavefunction, since tests with the 3-21G basis set showed that there was very little (<0.01 kcal/mol) decrease in energy and almost no geometry change after reoptimization was done using a broken-symmetry UHF singlet wavefunction, suggesting that an RHF description of these species is reasonable (Hehre *et al.*, 1986).

Frequencies and Isotope Effects. Frequency calculations were done on all stationary points. Ground states were found to have no imaginary frequencies, whereas transition states

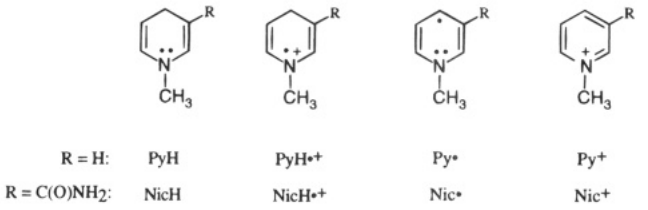

FIGURE 3: Ground-state species in the electron−proton−electron oxidation of *N*-methyl-1,4-dihydropyridine and *N*-methyl-1,4-dihydronicotinamide.

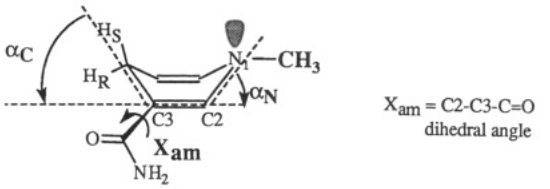

FIGURE 4: Atom and angle parameter definitions used in this paper for description of pyridines and nicotinamides. The angle αC is not dependent on the oxidation state, and the angle X_{am} is relevant only to nicotinamides.

were found to have a single imaginary frequency. A standard 0.89 scaling factor (Hehre *et al.*, 1986) was applied to frequencies used to calculate kinetic isotope effects. The kinetic isotope effects were calculated using QUIVER (Saunders *et al.*, 1989), which provides the partition functions for the Bigeleisen equation (Bigeleisen & Goeppert-Mayer, 1947).

For isotope effect ground-state frequencies, the two separate molecules which form the activated complex in the transition state were placed 25 Å apart, and a frequency calculation performed. The *independent* structures were fully optimized minima (proved by frequency calculations), but in the case of the *N*-methyl-1,4-dihydropyridine radical cation ($PyH^{\bullet+}$) and imidazole (Im), a small (127 cm^{-1}) imaginary frequency corresponding to a rotation of the methyl group was found when the two ground-state molecules were held at this distance. This was considered to be negligible in terms of the influence on the calculated isotope effect for deprotonation at C4, so it was ignored.

Electron Tunneling Pathway Calculations. A detailed description of similar electron tunneling pathway calculations, including a potential input file for NAD(P)H, is contained in an earlier paper (Almarsson *et al.*, 1993, including supplementary material), which also describes the same tunneling factors and driving force values used in this paper. The starting orbitals were (i) 214:TYR:OH-HL3, to determine coupling of the phenol oxygen lone pair of Tyr214 to Tyr357 or PP-IX, and (ii) NDP:C4-HQ3 and NDP:C4-HQ2, for determining coupling of dihydronicotinamide C4 hydrogens (H_R and H_S) to Tyr357 and Tyr214. The target orbitals were (i) 357:TYR:OH-HL3 and 357:TYR:OH-HQ9 (lone pairs on Tyr357), (ii) HEM:CBC-HQ23 (PP-IX vinyl group orbital near Tyr214), and (iii) 214:TYR:OH-HQ9 (the lone pair on the Tyr214 phenol oxygen nearest dihydronicotinamide C4). Paths involving lone pairs HQ9 and HL3 on Tyr214 had equal coupling if used as starting orbitals, since they are essentially the same distance from Tyr357 and PP-IX, but the lone pair HQ9 was better coupled to dihydronicotinamide C4. For mapping the coupling of the entire enzyme subunit, the goal orbital was the bond connecting iron to Tyr357 (HEM:NC-HL6).

RESULTS

Ab Initio Structures of Ground States and Transition States. The starting, intermediate, and product structures in the single-electron-transfer oxidation (eq 4) of *N*-methyl-1,4-dihydropyridine (PyH; see Figure 3 for structures) and *N*-methyl-1,4-dihydronicotinamide (NicH) were calculated using the 6-31G* basis set. The nicotinamide calculations were performed with the amide group in the *anti* conformation, which is the amide conformation found in the enzyme. In all four nicotinamide structures, the amide groups are rotated somewhat out of the plane of the ring. Amide groups of nicotinamides and dihydronicotinamides have been shown to have a flat energy potential surface for rotation about the C3−carbonyl carbon bond in the region where X_{am} (dihedral angle C2−C3−C=O; see Figure 4) is ~180° (Wu & Houk, 1993; Cummins & Gready, 1989). We assume this is the case for $NicH^{\bullet+}$ and $Nic^{\bullet}$ as well. Energies and geometrical parameters for the ground-state species in the EPE pathway (where ground-state species refers also to intermediate structures that lie in potential-energy minima) are listed in Table 1. The amide geometry and ring puckering into a pseudoboat conformation are similar to those previously reported (Almarsson *et al.*, 1993; Almarsson & Bruice, 1993; Wu *et al.*, 1994; Raber & Rodriguez, 1987), including the radical intermediate structures.

Transition structures were located for deprotonation of $PyH^{\bullet+}$ by hydroxide and imidazole and $NicH^{\bullet+}$ by imidazole (Figure 5). In both of the $PyH^{\bullet+}$ UHF/6-31G* transition structures (Table 1; Figure 5a,b) the dihydropyridine ring assumes a pseudoboat conformation, which results in pseudo-axial proton transfer from C4. In the UHF/6-31G* transition state for $NicH^{\bullet+}$ deprotonation (transition structure **3** ;Figure 5c and Figure 6), the bond lengths and angles about the transferring hydrogen ion are similar to those of **2** (Figure 5b). As with **1** and **2**, the ring assumes a pseudoboat conformation for proton transfer from C4. In **3**, (Im)C2−H forms a short contact (2.35 Å) with the amide oxygen. The starting geometry for this calculation was simply that of **2** with the amide group added in the *anti* conformation. During the transition-state optimization, the imidazole ring positioned as in **2** rotated by 61° about the forming (Im)N1−H′ bond; the amide group rotated to X_{am} = 142.9° (compared to the ground state, where X_{am} = 156.9°) in order to provide the geometry of **3**. The calculated electrostatic potential, mapped as color (where the spectrum from red to blue represents negative to positive electrostatic potential) onto a calculated electron isodensity surface, illustrates the attraction between the relatively electronegative lone pairs of the carbonyl and the relatively electropositive (Im)C2−H (Figure 6). This interaction appears to be a hydrogen bond [this interpretation is discussed at length by Derewenda *et al.* (1994) so is not repeated here]. Energetic and geometrical parameters for **3** are contained in Table 1.

Kinetic Isotope Effects (KIEs). Using the program QUIVER, scaled frequencies and the partition functions for the Bigeleisen equation were calculated at the desired temperature and with the desired isotopic substitution, using the force constants and geometry obtained from a quantum mechanical calculation. We calculated UHF/6-31G* frequencies for transition-state structures **1** and **2** as well as the separated reactants from **1** ($PyH^{\bullet+}$ + OH^-) and **2**($PyH^{\bullet+}$ + Im) and used these as input into QUIVER. Our calcula-

Table 1: *Ab Initio* Parameters for Dihydropyridine/Dihydronicotinamide Ground States and Transition States for Deprotonation[a]

structure	E (hartrees)	$\langle S^2 \rangle$	i (cm^{-1})	C−H (Å)	B−H (Å)	C−H−B (deg)	αN	βN	αC	X_{am}
PyH	−286.85190						5.0	28.4	2.6	
PyH$^{\bullet+}$(*vi*)	−286.63808	0.869								
PyH$^{\bullet+}$	−286.65437	0.874					0.5	2.2	0.1	
1	−362.20365	0.877	−2844.1[b]	1.342	1.247	175.7	7.6	24.3	10.0	
2	−511.45187	0.755	−2263.8[c]	1.408	1.318	178.0	2.9	6.4	9.9	
Py$^{\bullet}$	−286.26891	0.872					4.8	27.8	0.5	
Py^{+}(*vi*)	−286.08727									
Py^{+}	−286.10719						0	0	0	
NicH	−454.64173						1.7	4.9	3.1	155.7
NicH$^{\bullet+}$(*vi*)	−454.41981	0.844								
NicH$^{\bullet+}$	−454.43228	0.852					1.8	5.4	2.8	159.6
3[d]	−679.24214	0.787	−2244.3	1.347	1.383	176.2	2.7	1.8	10.5	142.9
Nic$^{\bullet}$	−454.05558	0.866					4.3	26.9	0.9	154.2
Nic^{+}(*vi*)	−453.86431									
Nic^{+}	−453.88393						0.5	1.1	1.6	150.9

[a] All are HF/6-31G* calculations as described in the text. B represents the oxygen or nitrogen atom which is acting as a base. X_{am}, αN, and αC (deg) are defined in Figure 4; βN is the pyramidalization (improper angle in degrees) about the ring nitrogen; CH_3 was always pseudoequatorial. Structures with no amide group were calculated in C_s symmetry; all nicotinamides were C_1 symmetry. The designation *vi* after a structure name indicates the energy of the vertically ionized state. [b] −2531.8 cm^{-1} following application of 0.89 scaling factor. [c] −2015.3 cm^{-1} following application of 0.89 scaling factor. [d] C−H- - -O hydrogen bond angle: 126.3°.

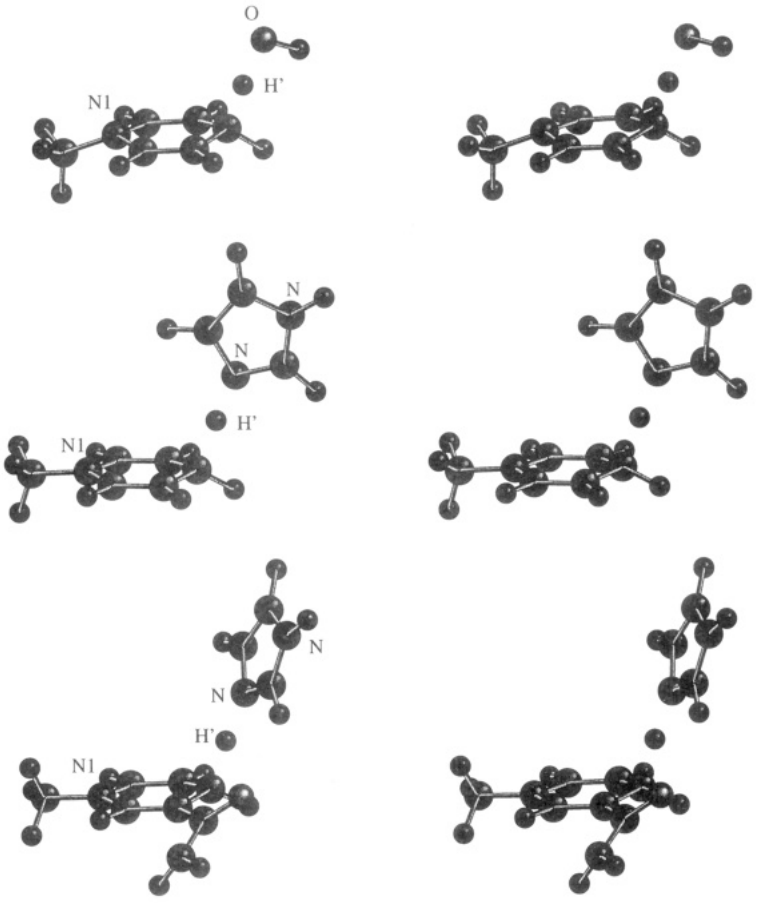

FIGURE 5: (a, top) Stereoview of UHF/6-31G* transition structure **1** (C_s symmetry) for deprotonation of PyH$^{\bullet+}$ by hydroxide ion. (b, middle) Stereoview of UHF/6-31G* transition structure **2** (C_s symmetry) for deprotonation of PyH$^{\bullet+}$ by imidazole. (c, bottom) Stereoview of UHF/6-31G* transition structure **3** (C_1 symmetry) for deprotonation of NicH$^{\bullet+}$ by imidazole. A short contact (2.35 Å) is formed between the amide carbonyl oxygen and the hydrogen attached to C2 of the imidazole ring.

tions give $k_H/k_{D2} = 5.83$ at 30 °C in the case of hydroxide as the base and $k_H/k_{D2} = 4.68$ at 30 °C with Im as the base. At 30 °C, the ZPE term was the dominant term in the Bigeleisen equation. Since the calculated Q_t^H of the Bell equation (Bell, 1980) was larger than the value (~5) deemed reasonable for a simple tunnel correction (Melander, 1960; Westheimer, 1961; Powell & Bruice, 1983), we chose not to apply tunneling corrections to the KIEs. The large magnitude of the imaginary frequency for proton transfer suggests that tunneling is important in these reactions, however.

Energetics of the EPE Pathway for Oxidation of NADH Models. The UHF/6-31G* calculated equilibria for deprotonation of PyH$^{\bullet+}$ by hydroxide and Im are quite different: the deprotonation step is strongly favored (−33.8 kcal/mol) with hydroxide as base, whereas deprotonation by Im is slightly disfavored (+2.2 kcal/mol). The exothermicity of deprotonation by hydroxide is due to the great stability of

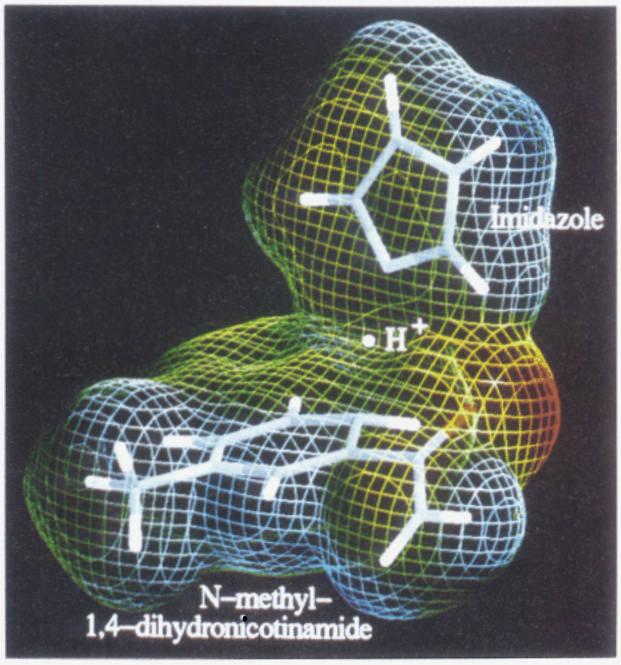

FIGURE 6: UHF/6-31G* transition structure for deprotonation of the *N*-methyl-1,4-dihydronicotinamide radical cation ($Nic^{\bullet+}$) by imidazole. The calculated electron isodensity surface (99.8% probability) and first-order electrostatic potential are shown as a colored grid surrounding the activated complex, where electronegative → electropositive zones span the spectrum from red → blue. The electron-rich amide oxygen lone pairs (red) are attracted to the electron-poor (blue) C2 hydrogen of imidazole. The transferring H^+ is buried in a region of intermediate (green) electrostatic potential.

water. The calculated activation energies for deprotonation of $PyH^{\bullet+}$ by different bases are comparable: 13.8 kcal/mol (hydroxide, Figure 5a) and 10.6 kcal/mol (Im, Figure 5b). After zero-point energy correction, the barrier heights are even closer, at 11.4 and 9.6 kcal/mol, respectively.

While proton abstraction from $PyH^{\bullet+}$ by Im is slightly disfavored, proton removal from $NicH^{\bullet+}$ by Im is calculated to be favorable (−3.9 kcal/mol). The difference is probably because the positive charge on $NicH^{\bullet+}$ is destabilized by the electron-withdrawing amide group . The calculated activation energy for deprotonation of $NicH^{\bullet+}$ by Im is only 2.1 kcal/mol. The hydrogen bond between the $NicH^{\bullet+}$ amide C=O and (Im)C2−H (see Figures 5c and 6) stabilizes the transition state relative to the reactants, which were calculated separately and received no hydrogen bond stabilization. The stabilizing effect of the (Im)C2−H hydrogen bond to the amide carbonyl in transition state **3** may be corrected for by estimating the strength of this interaction. We performed *ab initio* calculations at the RHF/6-31G* level on model systems (described below) which allow an estimate of the (Im)C2−H- - -O=C hydrogen bond strength as ~6 kcal/mol. After this correction was applied to the ground state, the barrier to deprotonation of $NicH^{\bullet+}$ by Im is ~8 kcal/mol. Zero-point energy correction (1.4 kcal/mol) lowers this barrier to ~7 kcal/mol.

Redox potentials have been shown (Tupper *et al.*, 1990; Wayner *et al.*, 1991; Danovich *et al.*, 1993) to be qualitatively reproduced by semiempirical and *ab initio* methods. This is particularly true in the case of closely related molecules and when the potential differences are on the order of 1 V (1 eV/particle = 23.06 kcal/mol). Ionization potentials correlate with electrochemical oxidation potentials

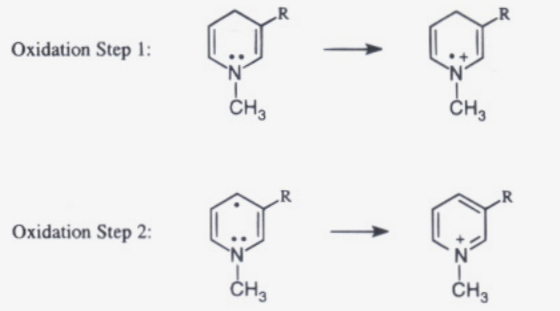

R = H { E_{ox} (Step 1) - E_{ox} (Step 2) = 0.88 V
E_{ox} (Step 1) - E_{ox} (Step 2) = 0.98 V (vertical ionization)

R = $C(O)NH_2$ { E_{ox} (Step 1) - E_{ox} (Step 2) = 1.01 V
E_{ox} (Step 1) - E_{ox} (Step 2) = 0.83 V (vertical ionization)

E_{ox} (Step 1) - E_{ox} (Step 2) = 1.65 V (experimental[a])

FIGURE 7: Comparison of calculated ionization potentials and electrochemical oxidation potentials for the first and second electron-removal steps in electron−proton−electron oxidation of PyH and NicH. Both the vertical and "relaxed" ionization potentials are reported. In all cases, the second oxidation is more facile than the first by a factor of >800 mV. Footnote *a*: electrochemical oxidation of *N*-benzyl-1,4-dihydronicotinamide (Fukuzumi *et al.*, 1987).

(Kavarnos & Turro, 1986). Ionization potentials were calculated for each of the single-electron oxidation steps in the EPE oxidation of PyH and NicH. This was done by calculation of the energy of the cations, both (i) at the geometry of the neutral species (in Table 1, these calculated energies are designated "*vi*" for "vertical ionization") and (ii) at their equilibrium geometry. Figure 7 illustrates how the neutral radicals $Nic^{\bullet}$ and $Py^{\bullet}$ are readily oxidized compared to the starting PyH or NicH molecules. The calculated results are in accord with experiments [e.g., Almarsson *et al.* (1993), Fukuzumi and Tokuda (1992), Fukuzumi *et al.* (1987), Sinha and Bruice (1984), Powell *et al.* (1984), Powell and Bruice (1983), and Moiroux and Elving (1980); see also references cited in these papers] which show that removal of the first electron is slower than removal of the second electron in EPE oxidation of NADH or NAD(P)H and analogues.

Imidazole C2−H Hydrogen Bonding with the Carbonyl Oxygen of NADH in X-ray and ab Initio Structures. The hydrogen attached to Cϵ of histidine [(His)Cϵ−H; which is comparable to (Im)C2−H] is the most acidic carbon-bound hydrogen in proteins, as was recently pointed out in a survey of histidines in protein X-ray crystal structures (Derewenda *et al.*, 1994). The study revealed a number of short contacts between (His)Cϵ−H and amide carbonyl oxygens, which were interpreted as hydrogen bonds. The calculated O−H distance in **5** (2.35 Å) is within the range of the X-ray observed distances (2.04−2.83 Å) of a variety of (His)Cϵ−H- - -amide carbonyl contacts listed by Derewenda *et al.* (1994).

We noticed that, using the X-ray coordinates of bovine catalase (Fita & Rossmann, 1985) and adding a hydrogen to Cϵ of His234, the distance between (His)Cϵ−H and the NAD(P)H amide oxygen is only 2.6 Å (assuming a trigonal-planar carbon atom and a 1.09 Å C−H bond). The C−H−O angle is 158°. To investigate this further, the X-ray coordinates of the heavy atoms of the Im ring of His234

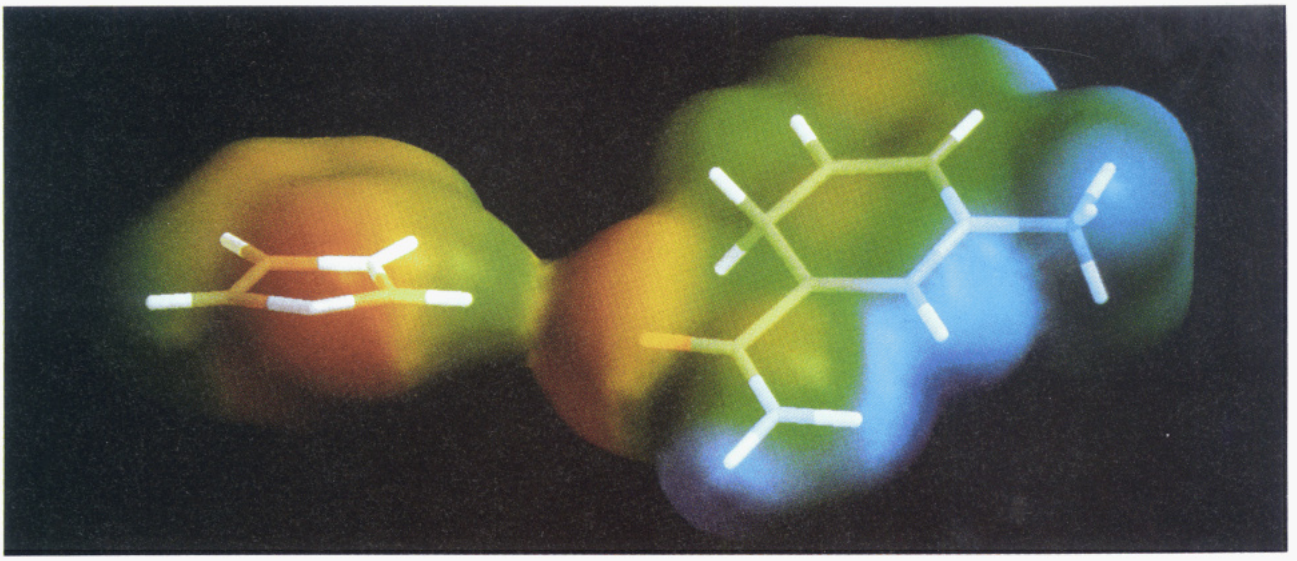

FIGURE 8: RHF/6-31G* single-point electron density and electrostatic potential shown as a colored surface (as in Figure 6, except as a solid surface rather than a grid) surrounding imidazole and NicH. The heavy atom locations were taken from the X-ray coordinates of the His234 imidazole ring and the NADPH dihydronicotinamide ring. There is electron overlap, with an approximately 2.6 Å distance from the carbonyl oxygen to the imidazole C2−H.

and of the nicotinamide portion of NAD(P)H were used to construct molecules of Im and NicH, juxtaposed in space precisely as in the enzyme crystal structure. Hydrogens were added without moving the heavy atoms. An RHF/6-31G* single-point calculation was then performed on this complex, followed by calculation of an electron density surface mapped with electrostatic potential (Figure 8). The calculated electron density shows O−H electron overlap, and the electrostatic potential in the overlap region suggests charge donation from the amide oxygen of NicH to (Im)C2−H.

We also performed geometry optimizations in which it was helpful to employ a model system which would not form competing N−H−N or N−H−O hydrogen bonds. Methyl groups were added to N1 of imidazole to give *N*-methylimidazole (NMI) and to the amide nitrogen of NicH (*cis* to the carbonyl) to give *N*,*N*′-dimethyl-1,4-dihydronicotinamide. Aside from these changes, the starting point was the crystal structure geometry as shown in Figure 8. RHF/3-21G optimization gave a structure (Figure 9a, Table 2) with a 2.24 Å H-O distance and 147.1° C−H−O angle. The calculations were time-consuming even with the 3-21G basis set, so the system was reduced to a more conveniently calculated complex of NMI with *cis*-*N*-methylformamide. The RHF/6-31G* hydrogen-bonded complex (Figure 9b, Table 2) has a 2.38 Å hydrogen bond, with a C−H−O angle of 171.0°. The calculation was begun in C_1 symmetry, but the structure converged to a C_s geometry. The energy lowering in this complex is 5.8 kcal/mol *vs* the separate molecules. This may be a reasonable approximate correction to apply to the reactants preceding transition state **3**. We have not calculated complexes of NMI with amide radical cations in order to determine if the strength of this type of interaction varies significantly with the oxidation state of the nicotinamide.

Calculation of Electron Tunneling Pathways in Catalase. Electron tunneling calculations (Beratan *et al.*, 1992; Onuchic *et al.*, 1992; Beratan *et al.*, 1991; Marcus & Sutin, 1985) were carried out to evaluate the various coupling elements ϵ between Tyr214, Tyr357, and the hydrogens attached to C4 of the dihydronicotinamide ring of NAD(P)H [see also

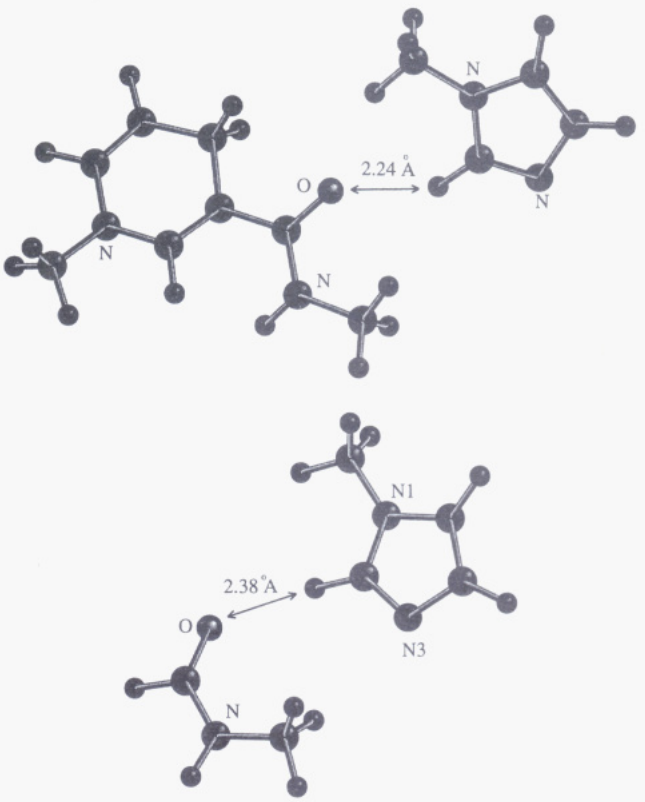

FIGURE 9: (a, top) RHF/3-21G optimized geometry of a C−H - - -O hydrogen-bonded complex between *N*-methylimidazole and *N*,*N*′-dimethyl-1,4-dihydronicotinamide. The starting point was the X-ray crystal structure geometry of the heavy atoms of the dihydronicotinamide ring of NAD(P)H and the imidazole ring of His234 as in Figure 8 which was, however, modified with methyl groups (for reasons described in the text) before optimization. (b, bottom) RHF/6-31G* optimized geometry of a C−H- - -O hydrogen-bonded complex between *N*-methylimidazole and *N*-methylformamide.

Almarsson *et al.* (1993)]. The best pathways are summarized in Table 3. The best direct tunneling routes from NAD(P)H to Tyr357 occurred *via* the PP-IX ring, using the same series of jumps as seen in the previous calculations (Figure 2a,b; Almarsson *et al.*, 1993), with only an additional short

Table 2: *Ab Initio* Energies and Symmetries of Amides, Bases, and Hydrogen-Bonded Complexes[a]

structure	*E* (hartrees)	symmetry
N-methylimidazole (NMI)	−263.84636	C_s
N-methylformamide (NMF)	−207.95961	C_1
complex of NMI + NMF[b]	−471.81526	C_s
imidazole	−244.81443	C_s
protonated imidazole	−225.19635	C_{2v}
hydroxide ion	−75.32659	$C_{\infty v}$
water	−76.01075	C_{2v}
N,*N*′-dimethyl-1,4-dihydronicotinamide + NMI (RHF/3-21G)		
	−753.30403	C_1

[a] All are RHF calculations and are with the 6-31G* basis set unless otherwise noted. [b] Calculation was begun in C_1 symmetry and converged within rounding error to a C_s result.

path through the porphyrin ring to the iron and then to Tyr357 (eq 5). Pathways were also calculated from Tyr214

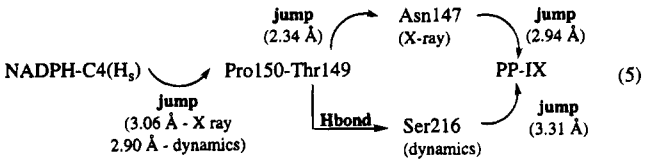

(5)

to Tyr357, following the suggestion of Hillar *et al.* (1994) that tyrosines may be implicated in radical migration. In the molecular dynamics structure of catalase (Almarsson *et al.*, 1993), the best path (Figure 10a, blue pathway) is *via* the porphyrin ring (eq 6). In the X-ray structure of catalase,

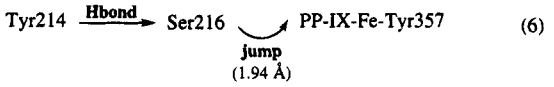

(6)

two nearly equivalent Tyr214−Tyr357 pathways exist (Figure 10b, purple and pink pathways), neither of which involves the porphyrin ring (eq 7). There is a strongly coupled

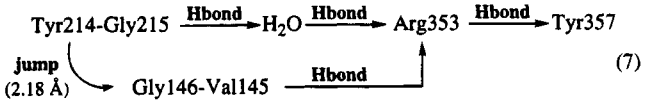

(7)

pathway between the porphyrin ring and Tyr214 calculated using the X-ray crystal structure (Figure 10b, blue pathway; eq 8). In both X-ray and molecular dynamics structures

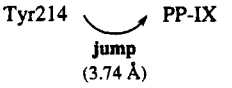

(8)

(Figure 10a,b; yellow pathways), the path between dihydronicotinamide C4−H_R is short (eq 9).

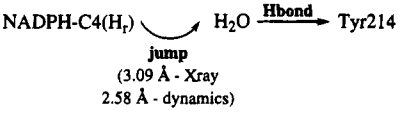

(9)

A map of the coupling of iron to the entire enzyme subunit was also created (Figure 11). The best coupling of any point on an amino acid or cofactor was taken as its overall coupling in constructing the map. Of the 20 tyrosine residues in each subunit of catalase, the most strongly coupled to iron were (1) Tyr357, which is directly ligated to the iron; (2) Tyr214, which bridges the PP-IX and NAD(P)H cofactors; and (3) Tyr235, which is also near both PP-IX and NAD(P)H. Table 4 lists the tyrosine residues in catalase and the log of ϵ for each one.

DISCUSSION

Electron−Proton−Electron (EPE) Pathway and Electron Tunneling in Catalase. Although there is ample experimental evidence [see, for example, Almarsson *et al.* (1993), Fukuzumi and Tokuda (1992), Fukuzumi *et al.* (1987), Powell *et al.* (1984), Sinha and Bruice (1984), Carlson *et al.* (1984), Powell and Bruice (1983), and Moiroux and Elving (1980); also references cited in these papers] in support of the accessibility of electron−proton−electron (EPE) (eq 4) transfer from NADH and analogues, this outlook is not without its critics. Hillar and Nicholls (1992) and Hillar *et al.* (1994), while recognizing that NAD(P)H bound to catalase "must act by somehow donating only one electron to regenerate a ferric state", reject an EPE mechanism for NAD(P)H oxidation (Almarsson *et al.*, 1993; Sinha & Bruice, 1984), proposing instead two-electron transfer with "concerted reduction of the ferryl iron and of a neighbouring protein free radical". Instantaneous loss of two electrons to form a dication [$NAD(P)H^{2+}$] must of course be immediately dismissed on grounds of electrochemical inaccessibility. Two-electron transfer via hydride can be dismissed, since

Table 3: Calculated Tunneling Matrix Elements ϵ[a] from PATHWAYS II Calculations

	ϵ values to targets[b]			
donor[b]	(1) heme vinyl	(2) Tyr357 (OH-HL3)	(3)Tyr357 (OH-HQ9)	(4) Tyr214 (OH-HQ9)
		X-Ray		
Tyr214	1.12×10^{-4} (12.1 Å)	4.64×10^{-6} (18.2 Å)	4.68×10^{-6} (18.4 Å)	
14-DHN(C4−H_S)	1.28×10^{-6} (13.2 Å)[d]	3.22×10^{-7} (18.8 Å)	3.22×10^{-7} (19.0 Å)	c
14-DHN(C4−H_R)	e	e	e	1.10×10^{-2} (3.9 Å)
		Dynamics		
Tyr214	9.84×10^{-5} (17.5 Å)	4.60×10^{-6} (25.0 Å)	4.60×10^{-6} (25.0 Å)	
14-DHN(C4−H_S)	1.22×10^{-5} (14.6 Å)[d]	1.58×10^{-6} (20.0 Å)	1.58×10^{-6} (20.0 Å)	c
14-DHN(C4−H_R)	e	e	e	6.00×10^{-3} (5.8 Å)

[a] See Almarsson *et al.* (1993) for the definition of coupling matrix element ϵ. See Figures 2 and 10 and the text for the pathways and their description. [b] The "Heme vinyl" target orbital was either CBC-HQ23 (in this work) or CAC-HQ22 [in table entries taken from Almarsson *et al.* (1993)]. The target orbital on Tyr214 was always OH-HQ9; the starting orbital was either OH-HQ9 or OH-HL3, which always had precisely equal coupling to a selected target. 14-DHN refers to the 1,4-dihydronicotinamide ring of NADPH. [c] Coupling to H_S, in this case, was inferior to H_r. [d] This table entry was taken from Almarsson *et al.* (1993). [e] Coupling to H_R, in this case, was inferior to H_S.

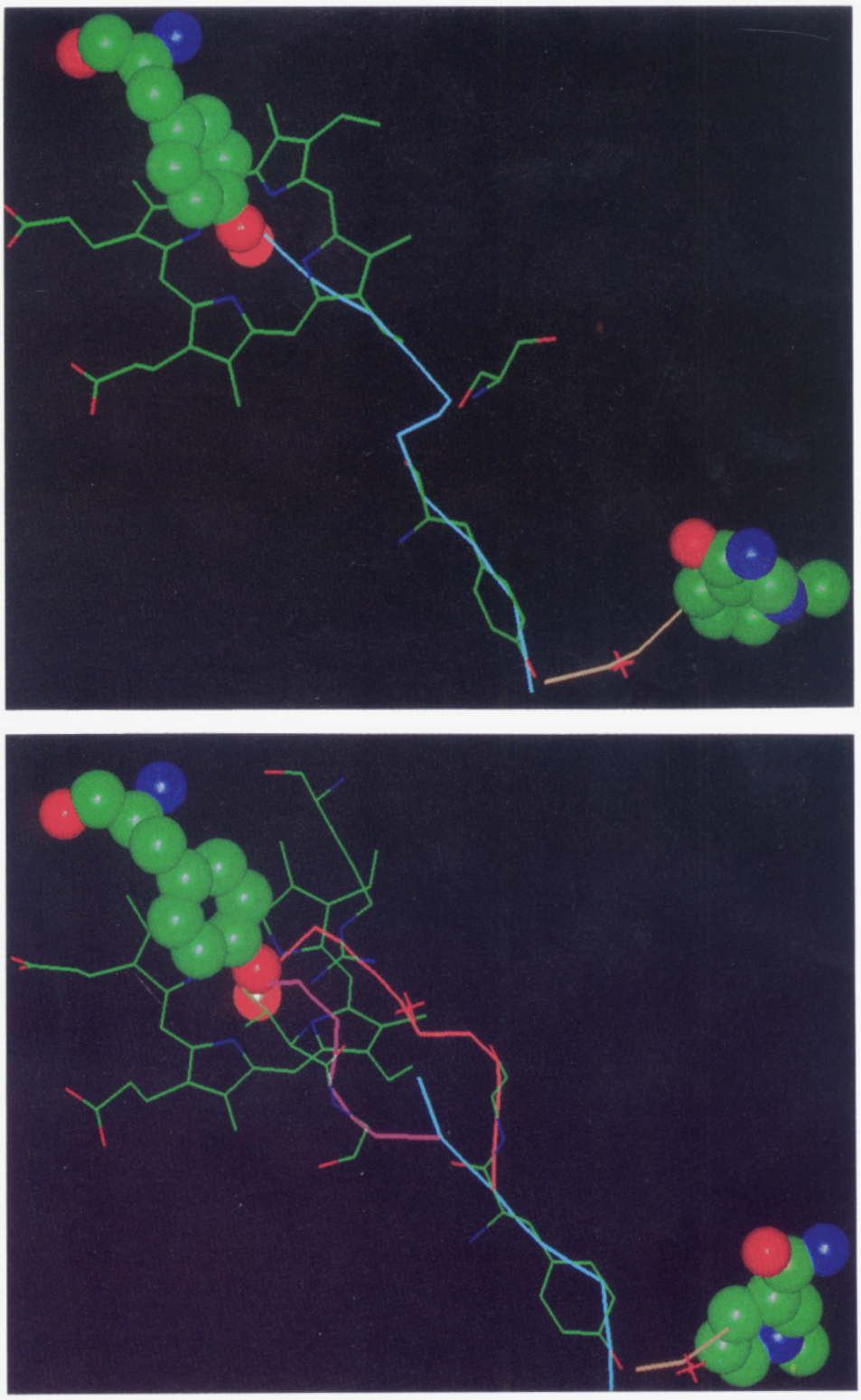

FIGURE 10: Calculated electron tunneling pathways based on the molecular dynamics structure (a, top) and X-ray crystal structure (b, bottom) of bovine catalase. The 1,4-dihydronicotinamide ring of NADPH and the amino acid residue Tyr357 are depicted as space-filling models. The yellow lines represent the best pathways between NAD(P)H C4(H_r) and Tyr214 (eq 9 in text). In panel a, the blue line is the best pathway from Tyr214 to Tyr357 (eq 6 in text). In panel b, the blue line represents the best pathway from Tyr214 to protoporphyrin IX (eq 8 in text); the purple and pink lines are separate pathways (eq 7 in text) of nearly equal coupling between Tyr214 and Tyr357. The latter three paths overlap each other for part of their distance.

the distance from NAD(P)H to the porphyrin is too far (Figure 1) for such transfer. The same reasoning disallows direct $H^{\bullet}/e^{-}$ transfer, which would be stepwise in any case [see Tanner *et al.* (1989) for an example]. There seems little basis to insist that two electrons departing the NAD(P)H in a concerted way are inherently "more parsimonious, and therefore more acceptable" (Hillar *et al.*, 1994), than a relatively simple, well-precedented EPE pathway.

There is the possibility of a redox pathway which depends upon relocation of electron deficiency to a site nearer the NAD(P)H. Evidence exists (Chuang & Van Wart, 1992; Thanabal *et al.*, 1988; Fujita *et al.*, 1983) that the electron

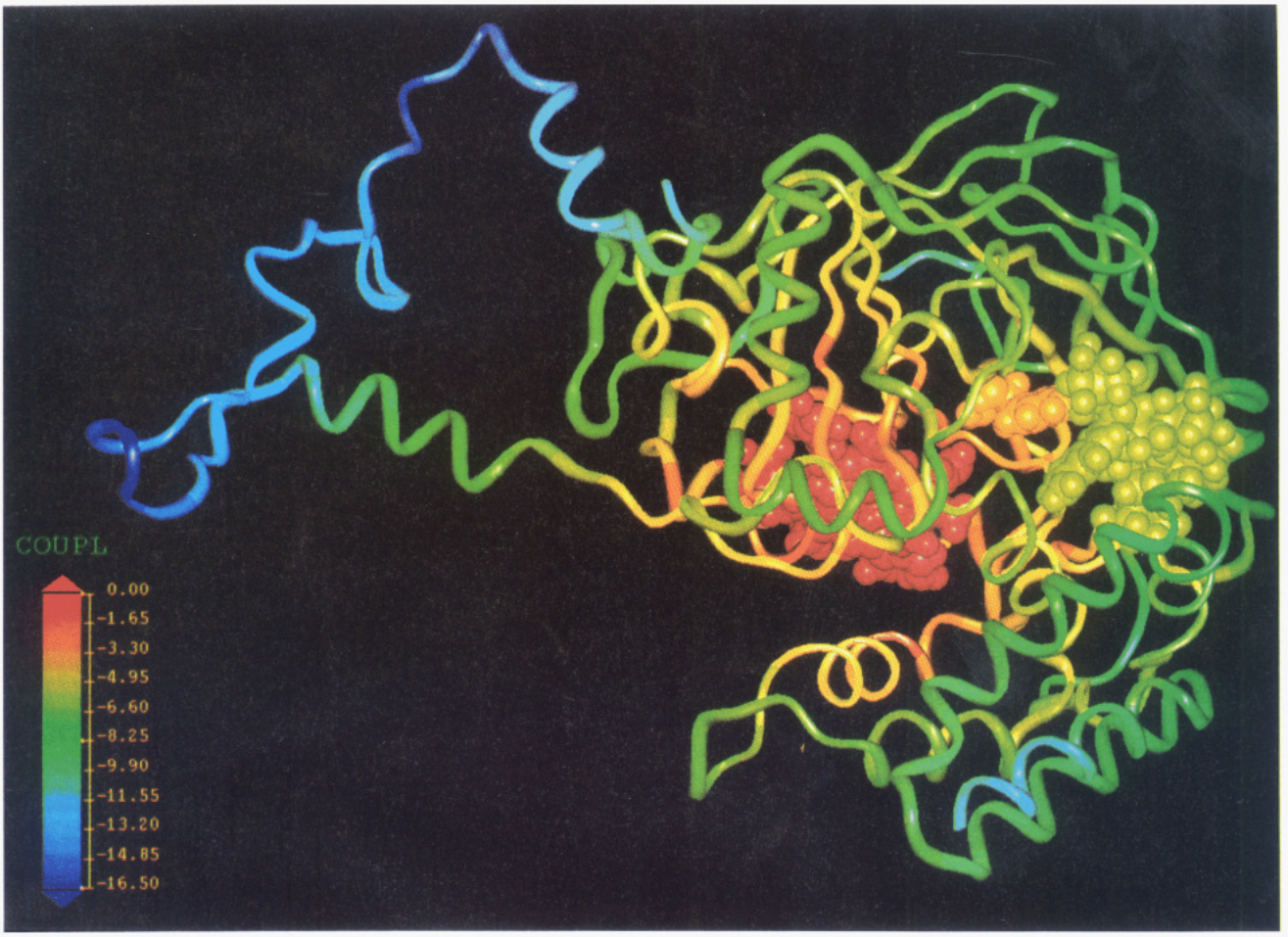

FIGURE 11: Coupling map of catalase, where the peptide backbone is depicted in a ribbon representation. The cofactors NAD(P)H and iron-protoporphyrin IX, as well as tyrosine residues 214 and 357, are depicted as space-filling models. The colors of all amino acids and cofactors reflect donor−acceptor coupling to the iron atom, with the scale at the left indicating the strength of coupling, where the coupling matrix element $\epsilon = 10^x$ (x taken from scale). The strongest coupling of any point on an amino acid residue to iron is taken as that residue's overall coupling, and the peptide backbone is colored accordingly.

Table 4: Coupling Matrix Elements ϵ for Tyrosine Residues in Catalase[a]

	log ϵ			log ϵ	
residue no.	X-ray	dynamics	residue no.	X-ray	dynamics
83	−6.23	−5.90	324	−4.75	−3.69
93	−7.85	−7.09	357	−0.75	−0.22
136	−5.85	−5.33	369	−4.08	−3.49
214	−3.06	−3.12	378	−6.79	−6.11
230	−5.72	−4.85	385	−9.63	
235	−3.88	−4.24	403	−11.38	
259	−6.50	−5.56	404	−12.05	
273	−7.79	−7.15	446	−7.65	−7.81
279	−5.62	−5.59	488	−6.83	−7.53
307	−6.97	−7.14	499	−10.62	−8.85

[a] Tyrosine residues 385, 403, and 404 are part of the hinge peptide region which was not included in the molecular dynamics structure [see Almarsson *et al.*, (1993)].

deficiency of the porphyrin π-cation radical of compound **I** is likely delocalized onto the proximal Tyr357 ligand in catalase. If the electron-deficient Tyr357 oxidizes, for example, an exogenous oxidant, the enzyme is in danger of deactivation. If the electron deficiency were to migrate [as was suggested by Hillar *et al.* (1994)], to Tyr214, the oxidized phenolic oxygen would reside ~4−6 Å from C4 of the dihydronicotinamide ring of bound NAD(P)H (Figure 10). A secondary tunneling event (Figure 10) might oxidize NAD(P)H to NAD(P)H$^{\bullet+}$.

How likely is it that Tyr214 would be oxidized before NAD(P)H? As seen in Table 3, this residue is more strongly coupled (higher ϵ value) to the iron PP-IX−Tyr357 moiety than is NAD(P)H. Furthermore, the oxidation potentials of phenols (Stradlins & Hasanli, 1994) and tyrosine (Harriman, 1987) exhibit a dramatic pH dependence, as does the rate of long-range electron-transfer oxidation of tyrosines in model oligopeptides (Mishra *et al.*, 1994). Such a pH dependence is also seen in catalysis by phenols or tyrosine of the one-electron oxidation of NADH by ferricyanide or ferricytochrome *c* (Sherman *et al.*, 1989). It is reasonable to assume that tyrosine, in its anionic state, would be more easily oxidized than NAD(P)H, since the oxidation potential (*vs* SCE) for *p*-methylphenoxide is 0.2 V (Stradlins & Hasanli, 1994), whereas for *N*-benzyl-1,4-dihydronicotinamide, it is 0.6 V (Fukuzumi *et al.*, 1987). As was pointed out by Mishra *et al.* (1994), it has been known for many years that local environments in proteins can strongly influence pK_a's of tyrosine residues (Tanford *et al.*, 1955). In the X-ray crystal structure of catalase, an Asp212 carboxyl oxygen is only 3.6 Å, and a water molecule [which is surrounded by His234, His304, and a phosphate oxygen of the NAD(P)H diphosphate linkage] is only 2.7 Å from the Tyr214 phenol oxygen. This environment may be basic enough to deprotonate the phenol, at least long enough in order that electron transfer may occur. Equation 10 provides two plausible

mechanistic schemes which involve tyrosines in electron transfer from NAD(P)H:

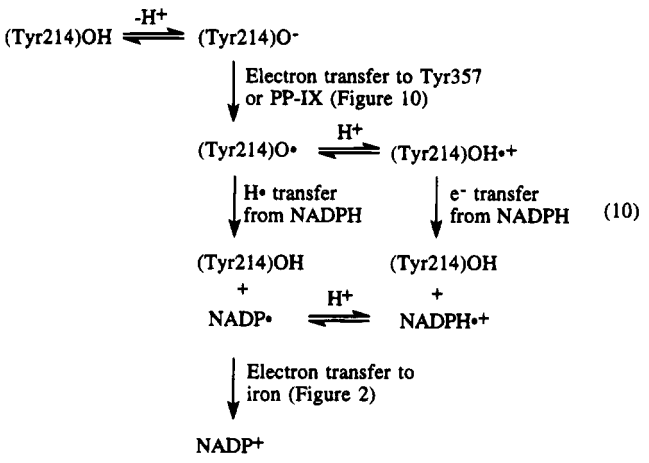

This equation encompasses the two most reasonable possibilities for electron transfer in catalase if Tyr214 is involved. It has been recently shown (Foti *et al.*, 1994) that phenol radicals abstract H• from some donors at an unexpectedly high rate, so it is possible that H• transfer would produce NADP• from NAD(P)H. However, the proximity of the basic residues His234 and His304 to C4 of the nicotinamide ring finds easiest explanation in the supposition that they play a role as general bases to convert NAD(P)H$^{\bullet+}$ generated in an EPE mechanism to NADP• (eq 11). The

$$\text{NAD(P)H}^{\bullet+} + \text{His} \rightarrow \text{NADP}^{\bullet} + \text{HisH}^{+} \qquad (11)$$

second redox step would involve e^- transfer from NADP• to the iron(IV) oxo porphyrin to regenerate the iron(III) state. This e^- transfer must involve tunneling pathways such as shown in Figure 2.

In our tunneling calculations, Tyr357 was more weakly coupled to the reductants Tyr214 and NAD(P)H than was the porphyrin ring. Indeed, except for the case of electron transfer from Tyr214 to Tyr357 using the X-ray crystal structure, the best route for tunneling was via the porphyrin ring. This is not to assert that pathways involving Tyr357 are not important; there is evidence (Chuang & van Wart, 1992; Thanabal *et al.*, 1988; Fujita *et al.*, 1983) that electron deficiency resides on this residue in compound **I**, and electrons must, of course, migrate to a site of electron deficiency even if the coupling is not strong.

Experiments on model systems (Almarsson *et al.*, 1993; Fukuzumi *et al.*, 1992; Sinha & Bruice, 1984; Carlson *et al.*, 1984; Powell & Bruice, 1983) show that the rate-determining step in EPE oxidation of NADH analogues depends on the strength of the oxidant. With strong oxidants such as ferricyanide, deprotonation of the intermediate radical cation is rate-determining, whereas with a weaker oxidant such as ferrocenium, initial electron transfer is the slow step. In catalase, it is unknown whether electron tunneling (Figure 2 and/or 10) might be slow compared to proton transfer from the radical cation.

Deprotonation Transition State Structure and Kinetic Isotope Effects. Anisotropic puckering of the dihydronicotinamide ring into a pseudoboat conformation has been observed in the ground-state molecular dynamics calculations of the dihydronicotinamide cofactors in catalase and dehydrogenase (Almarsson *et al.*, 1993; Almarsson & Bruice, 1993).

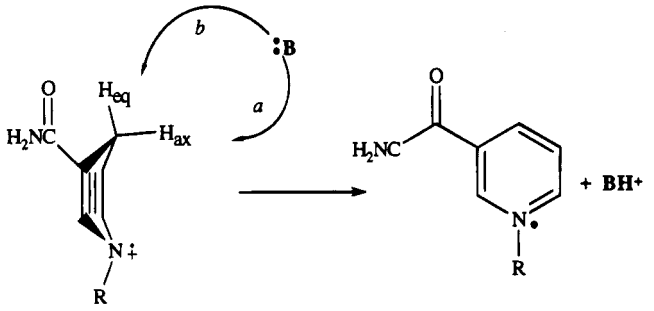

FIGURE 12: Two possible routes of attack by a base to deprotonate NicH$^{\bullet+}$. Pseudoaxial attack (*a*) is favored over pseudoequatorial attack (*b*).

1993). We also now observe puckering in *ab initio* transition structures for deprotonation for Nic$^{\bullet+}$ and PyH$^{\bullet+}$. The transition structures **1**, **2**, and **3** are similar, with respect to ring conformation and C−H′ distance, to those calculated for hydride transfer from neutral dihydropyridine and dihydronicotinamide cofactors (Wu & Houk, 1987; Wu *et al.*, 1995; Cummins & Gready, 1990). As has been suggested previously, ring puckering to deliver a hydrogen ion from a pseudoaxial position on the dihydronicotinamide ring (Figure 12) appears to provide a kinetic advantage, assisting in the departure of the hydrogen ion (Almarsson *et al.*, 1993; Almarsson & Bruice, 1993).

In the X-ray crystal structure of bovine catalase, the imidazole bases His234 and His304, as well as a molecule of water, reside near C4 of the nicotinamide ring (Figure 13) in the NAD(P)H binding site. The distance of nicotinamide C4 to the His304 nitrogen is 4.2 Å [a difference of only 1.5 Å from the ground state compared to transition state **3**, where the (NicH$^{\bullet+}$)C4 to (Im)N1 distance is 2.7 Å]. An imidazole nitrogen of His304 is only 3.3 Å from dihydronicotinamide H_R and 4.6 Å from H_s. Meanwhile, an imidazole nitrogen of His234 is 5.0 Å from H_R and 5.1 Å from H_s, which appears to be a poorer interaction. Contrary to this, however, our earlier molecular dynamics simulations of catalase (Almarsson *et al.*, 1993) suggested that the time-averaged structure places His234 in a preferred position for deprotonation at H_r, with other combinations of histidines and C4 hydrogens less favorable. As another possibility, the general base may be the water molecule bound near C4, with protons then rapidly shuttled away to either His234 or His304.

Kinetic isotope effects (KIEs) are among the few experimental observables which can provide information concerning transition-state structure. Isotope effects have been measured for the EPE mechanism of $Fe(CN)_6^{3-}$ oxidation of *N*-methyl-10,10-dihydroacridan (MAH) and *N*-methyl-10,10-dideuterioacridan (MAD) radical cations by a variety of bases (Sinha & Bruice, 1984; Almarsson *et al.*, 1993). It was found that k_H/k_{D2} = 7−10, 4.6, 5.4, and 5.6 for deprotonation at 30 °C by water, formate, acetate, and imidazole, respectively. These data were interpreted as showing that in the EPE mechanism (i) proton transfer from MAH$^{\bullet+}$ constitutes the rate-determining step, (ii) the transition state for proton transfer is early, and (iii) moderate tunneling plays a role in the KIE. Our calculated KIEs for deprotonation of PyH$^{\bullet+}$ (k_H/k_{D2} = 5.83 at 30 °C with hydroxide base and k_H/k_{D2} = 4.68 at 30 °C with Im as the base) with zero and two deuteriums attached to C4 of the dihydropyridine ring are similar enough to the MAH$^{\bullet+}$/

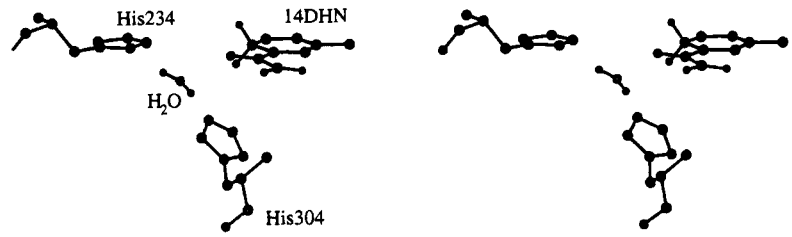

FIGURE 13: Stereoview of imidazole bases His234 and His304 and a bound water molecule near C4 of the 1,4-dihydronicotinamide ring (14DHN) of NAD(P)H.

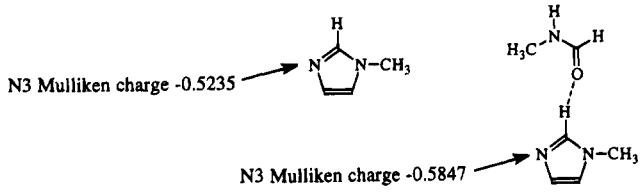

FIGURE 14: RHF/6-31G* calculated Mulliken charges on N3 of *N*-methylimidazole in the isolated molecule and its C−H- - -O hydrogen-bonded complex with *N*-methylformamide.

$MAD^{\bullet+}$ isotope effects to suggest that the UHF/6-31G* calculations reasonably reproduce transition-state as well as ground-state structure and support the interpretation (Sinha & Bruice, 1984; Almarsson *et al.*, 1993) explaining experimental KIEs in the $MAH^{\bullet+}/MAD^{\bullet+}$ system (i, ii, and iii, *loc. cit.*).

Implications of Hydrogen Bonding of Imidazole C2−H with the Carbonyl Oxygen. Since imidazole nitrogens of both His234 or His304 are near nicotinamide C4, we cannot simply use proximity to favor one or the other histidines acting as the base responsible for deprotonation of $NAD(P)H^{\bullet+}$. Another factor may come into play, however. In the case of deprotonation of $NAD(P)H^{\bullet+}$ by an imidazole, it may be that there is a "push−pull" effect in which electron density accepted from the amide carbonyl by (Im)C2−H increases basicity at (Im)N1, assisting deprotonation from C4 of the nicotinamide ring. Such a phenomenon *might* be seen in transition state **3** (Figures 5c and 6), which has a lower calculated barrier to deprotonation (~7 kcal/mol) than does transition state **2** (Figure 5b), which has a 9.6 kcal/mol barrier [there may be some doubt on this point, due to uncertainty in the precise strength of the C−H- - -O hydrogen bond and the possibility that the level of UHF spin contamination (Table 1) may alter the energetics; ideally, one would like to include solvent effects and electron correlation in the *ab initio* calculations; this might alter the relative barrier heights]. Analysis of the charge distribution in a model system supports the possibility of such an effect. The RHF/6-31G* Mulliken charge at N3 of *N*-methylimidazole is −0.5235 in the isolated molecule; in its hydrogen-bonded complex with *N*-methylformamide, the charge on this atom increases by 12%, to −0.5847 (Figure 14). This may be reflected in greater basicity at that site, and a similar phenomenon may occur in histidines with (Im)C2−H hydrogen bonds to carbonyl oxygens. This latter possibility was suggested by Derewenda *et al.* (1994), who analyzed crystal structures of a number of serine proteases. The study showed that, invariably, histidines in the active sites of serine proteases had the imidazole C2−H of histidine (of the Ser-His-Asp "catalytic triad" of amino acid residues) in close contact with amide carbonyls of a nearby polypeptide chain. Only 15% of non-active-site histidines showed such contacts. The fact that this interaction was highly conserved in the active site was taken as evidence for a likely catalytic role, *via* alteration of the electron demand of the imidazole ring of histidines. It seems likely to us that the C−H- - -O hydrogen bond influences "low-barrier" hydrogen bonds (Frey et al., 1994) in such a way as to assist catalysis in serine proteases. We now observe C−H- - -O hydrogen-bonding interactions between histidine or imidazole and amide carbonyl oxygens of dihydronicotinamides in *ab initio* calculated structures and the X-ray crystal structure (Fita & Rossmann, 1985) of bovine catalase. If charge donation through such a hydrogen bond creates a "push−pull" effect in bovine catalase, the likelihood that His234 deprotonates $NAD(P)H^{\bullet+}$ may be greater than would otherwise be supposed.

ACKNOWLEDGMENT

We thank Dr. Örn Almarsson, Ms. Felice Lightstone, and Mr. Kenneth Browne for helpful discussions.

REFERENCES

Almarsson, Ö., & Bruice, T. C. (1993) *J. Am. Chem. Soc. 115*, 2125−2138.
Almarsson, Ö., Sinha, A., Gopinath, E., & Bruice, T. C. (1993) *J. Am. Chem. Soc. 115*, 7093−7102.
Barry, B. A., & Babcock, G. T. (1987) *Proc. Natl. Acad. Sci. U.S.A. 84*, 7099−7103.
Bell, R. P. (1980) *The Tunnel Effect in Chemistry*, Chapman and Hall, London.
Bender, C. J., Sahlin, M., Babcock, G. T., Barry, B. A., Chandrasekhar, T. K., Salowe, S., Stubbe, S., Lindstrom, B., Petersson, L., Ehrenberg, A., & Sjoberg, B. M. (1989) *J. Am. Chem. Soc. 111*, 8076−8083.
Beratan, D. N., Betts, N. J., & Onuchic, J. N. (1991) *Science 252*, 1285−1288.
Beratan, D. N., Onuchic, J. N., Winkler, J. R., & Gray, H. B. (1992) *Science 258*, 1740−1741.
Bigeleisen, J., & Goeppert-Mayer, M. (1947) *J. Chem. Phys. 15*, 261−267.
Bigeleisen, J., & Wolfsberg, M. (1958) *Adv. Chem. Phys. 1*, 15−64.
Biosym Inc. (1992) *Insight II software version 2.20*, San Diego, CA.
Carlson, B. W., Miller, L. L., Neta, P., & Grodkowski, J. (1984) *J. Am. Chem. Soc. 106*, 7233−7239.
Chandrasekhar, T. K., O'Malley, P. J., Rodriguez, I., & Babcock, G. T. (1986) *Photosynth. Res. 10*, 423−429.
Chuang, W.-J., & van Wart, H. E. (1992) *J. Biol. Chem. 267*, 13293−13301.
Clark, T. (1985) *A Handbook of Computational Chemistry*, Wiley, New York.
Cummins, P. L., & Gready, J. E. (1989) *THEOCHEM 183*, 161−174.
Cummins, P. L., & Gready, J. E. (1990) *J. Comput. Chem. 11*, 791−804.
Danovich, D., & Apeloig, Y., & Shaik, S. (1993) *J. Chem. Soc., Perkin Trans. 2*, 321−330.
Derewenda, Z. S., Derewenda, U., & Kobos, P. M. (1994) *J. Mol. Biol. 241*, 83−93.

Dewar, M. J. S., & Merz, K. M. (1985) *J. Am. Chem. Soc. 107*, 3902−3909.
Dolphin, D., Forman, A., Borg, D. C., Fajer, J., & Felton, R. H. (1971) *Proc. Natl. Acad. Sci. U.S.A. 68*, 614−618.
Fita, I., & Rossmann, M. G. (1985) *Proc. Natl. Acad. Sci. U.S.A. 82*, 1604−1608.
Foti, M., & Ingold, K. U., & Lusztyk, J. (1994) *J. Am. Chem. Soc. 116*, 9440−9447.
Frey, P. A., Whitt, S. A., & Tobin, J. B. (1994) *Science 264*, 1927−1930.
Frisch, M. J., Trucks, G. W., M. Head-Gordon, M., Gill, P. M. W., Wong, M. W., Foresman, J. B., Johnson, B. G., Schlegel, H. B., Robb, M. A., Replogle, E. S., Gomperts, R., Andres, J. L., Raghavachari, K., Binkley, J. S., Gonzalez, C., Martin, R. L., Fox, D. J., Defrees, D. J., Baker, J., Stewart, J. J. P., & Pople, J. A. (1992) *Gaussian 92, Revision E.2*, Gaussian, Inc., Pittsburgh, PA.
Fujita, I., Hanson, L. K., Walker, F. A., & Fajer, J. (1983) *J. Am. Chem. Soc. 105*, 3296−3300.
Fukuzumi, S., & Tokuda, Y. (1992) *Chem. Lett.*, 1721−1724.
Fukuzumi, S., Koumitsu, S., Hironaka, K., & Tanaka, T. (1987) *J. Am. Chem. Soc. 109*, 305−316.
Gråslund, A.; Ehrenberg, A., & Thelanders, L. J. (1982) *J. Biol. Chem. 257*, 5711−5715.
Harriman, A. (1987) *J. Phys. Chem. 91*, 6102−6104.
Hehre, W. J., Radom, L., Schleyer, P. v. R., & Pople, J. A. (1986) *Ab initio Molecular Orbital Theory*, Wiley, New York.
Hillar, A., & Nicholls, P. (1992) *FEBS Lett. 314*, 179−182.
Hillar, A., Nicholls, P., Switala, J., & Loewen, P. C. (1994) *Biochem. J. 300*, 531−539.
Jouve, H. M., Beaumont, F., Leger, I., Foray, J., & Pelmont, J. (1989) *Biochem. Cell Biol. 67*, 271−277.
Kavarnos, G. J., & Turro, N. J. (1986) *Chem. Rev. 86*, 401−449.
Kirkman, H. N., & Gaetani, G. F. (1984) *Proc. Natl. Acad. Sci. U.S.A. 81*, 4343−4347.
Kirkman, H. N., Galiano, S., & Gaetani, G. F. (1987) *J. Biol. Chem. 262*, 660−666.
Kulmacz, R. J., Tsai, A. L., & Palmer, G. (1987) *J. Biol. Chem. 262*, 10524−10531.
Marcus, R. A., & Sutin, N. (1985) *Biochim. Biophys. Acta 811*, 265−322.
Melander, L. (1960) *Isotope Effects on Reaction Rates*, Ronald Press, New York.
Melyik-Adamyan, W. R., Barynin, V. V., Vagin, A. A., Borisov, V. V., Vainshtein, B. K., Fita, I., Murphy, M. R. N., & Rossmann, M. G. (1986) *J. Mol. Biol. 188*, 63−72.
Mishra, A. K., Chandrasekhar, R., Faraggi, M., & Klapper, M. H. (1994) *J. Am. Chem. Soc. 116*, 1414−1422.
Moiroux, J., & Elving, P. J. (1980) *J. Am. Chem. Soc. 102*, 6533−6538.
Moss, T. H., Ehrenberg, A., & Beardon, A. J. (1969) *Biochemistry 8*, 4159−4162.
Murthy, M. R. N., Reid, T. J., III, Sicignan, A., Tanaka, N., & Rossmann, M. G. (1981) *J. Mol. Biol. 152*, 465−499.
Onuchic, J. N., Beratan, D. N., Winkler, J. R., & Gray, H. B. (1992) *Annu. Rev. Biophys. Biomol. Struct. 21*, 349−377.
Powell, M. F., & Bruice, T. C. (1983) *J. Am. Chem. Soc. 105*, 7139−7149.
Powell, M. F., Wu, J. C., & Bruice, T. C. (1984) *J. Am. Chem. Soc. 106*, 3850−3856.
Regan, J. J. (1993) *PATHWAYS II software, version 2.01*, University of California−San Diego, San Diego, CA.
Roberts, J. E., Hoffman, B. M., Rutter, R., & Hager, L. P. (1981) *J. Biol. Chem. 256*, 2118−2121.
Saunders, M., Laidig, K. E., & Wolfsberg, M. (1989) *J. Am. Chem. Soc. 111*, 8989−8994.
Schmidt, M. W., Baldridge, K. K., Boatz, J. A., Elbert, S. T., Gordon, M. S., Jensen, J. H., Koseki, S., Matsunaga, N., Nguyen, K. A., Su, S. J., Windus, T. L., Dupuis, M., & Montgomery, J. A., (1993) *GAMESS Version = 4 Mar 1993*, Iowa State University, Ames, IA.
Schonbaum, G. R., & Chance, B. (1976) in *The Enzymes* (Boyer, P. D., Ed.) 2nd ed., Vol. 13, pp 363−408 Academic Press, New York.
Schulz, C. E., Devaney, P. W., Winkler, H., Debrunner, P. G., Doan, N., Chiang, R., Rutter, R., & Hager, L. P. (1979) *FEBS Lett. 103*, 102−105.
Sherman, G. W., Frothingham, G. K., & Howland, J. L. (1989) *Biochem. Arch. 5*, 339−343.
Sinha, A., & Bruice, T. C. (1984) *J. Am. Chem. Soc. 106*, 7291−7292.
Tanford, C., Hauenstein, J. D., & Rands, D. G. (1955) *J. Am. Chem. Soc. 77*, 6409−6413.
Tanner, D. D., & Kharrat, A., & Mahamat-Oumar, H. (1990) *Can. J. Chem. 68*, 1662−1667.
Thanabal, V., La Mar, G. N., & de Ropp, J. S. (1988) *Biochemistry 27*, 5400−5407.
Tupper, K. J., Davidson, E. R., & Gajewski, J. J. (1990) *Theor. Chim. Acta 78*, 25−30.
Vainshtein, R. K., Melik-Adamyan, W. R., Barynin, V. V., Vagin, A. A., Grebrenko, A. I., Borisov, V. V., Bartels, K. S., Fita, I., & Rossmann, M. G. (1986) *J. Mol. Biol. 188*, 49−61.
Wavefunction Inc. (1994) *Spartan 3.1 software*, 18401 von Karman Ave., Irvine, CA.
Wayner, D. D. M., Sim, B. A., & Dannenberg, J. J. (1991) *J. Org. Chem. 56*, 4853−4858.
Westheimer, F. H. (1961) *Chem. Rev. 61*, 265−273.
Whittaker, M. M., & Whittaker, J. W. (1990) *J. Biol. Chem. 265*, 9610−9613.
Wolfsberg, M., & Stern, M. (1964) *Pure Appl. Chem. 8*, 225−232.
Wu, Y.-D., & Houk, K. N. (1991) *J. Am. Chem. Soc. 113*, 2353−2358.
Wu, Y.-D., & Houk, K. N. (1993) *J. Org. Chem. 58*, 2043−2045.
Wu, Y.-D., Lai, D. K. W., & Houk, K. N. (1995) *J. Am. Chem. Soc. 117*, 4100−4108.

BI942870X